Geometry of locomotion of the generalized Purcell's swimmer : Modelling and controllability

Sudin Kadam, Ravi Banavar

arXiv:1611.05154v1 [cs.RO] 16 Nov 2016

***Abstract*—Micro-robotics at low Reynolds number has been a growing area of research over the past decade. We propose and study a generalized 3-link robotic swimmer inspired by the planar Purcell's swimmer at low Reynolds number. By incorporating out-of-plane motion of the outer limbs, this mechanism generalizes the planar Purcell's swimmer, which has been widely studied in the literature. Such an evolution of the limbs' motion results in the swimmer's base link to evolve in a 3 dimensional space. This swimmer's configuration space admits a trivial principal fiber bundle structure, which along with the slender body theory at the low Reynolds number regime, facilitates obtaining a kinematic form of the equations. A coordinate-free expression for the local form of the kinematic connection is then derived, followed by a local parametrization for simulation purpose. We then present a local controllability analysis of the swimmer in the low Reynolds number regime using weak controllability results of the planar Purcell's swimmer.**

***Index Terms*—Micro-robotics, Purcell's swimmer, low Reynolds number swimming, kinematic modelling, nonlinear controllability, principal fiber bundle.**

I. Introduction

Locomotion is one of the most crucial activities for the existential requirements of microbial and animal life. For robots or living organisms it is related to body movements that results in transportation from a physical place to another. There are two major goals in this field - to understand the mechanics of locomotion of existing biological systems, and to devise mobile robotic systems to perform certain desired objectives, possibly by mimicking these biological systems. A commonality in most of the approaches in locomotion is the periodic variation in limbs or shape variables to achieve macroscopic motion. This idea of undulatory limb motion to produce a macroscopic motion is observed in many biological systems from motile microbes to swimming snakes. The idea also appears in a number of engineering settings as presented in [1] [2], [3], [4], [5].

The interaction with the environment to achieve the motion forms a key to analysis of locomoting systems. Most of our intuition about locomotion originates from inertia-dominant systems used by larger animals. As opposed to such systems, micro-organisms resort to a creeping motion. The usual mechanism for swimming in water for larger animals involves obtaining a forward momentum from the surrounding fluid due to some periodic body motion. The effect of inertia is that the displacement gained in the first half period of a cyclic motion is not cancelled out by that of the second half period [6]. Such a mechanism, however, does not work in the microscopic world of biological objects where the inertia is negligible and viscosity dominates the motion. This effect is observed at very low Reynolds numbers, which is the ratio of the inertial to viscous forces acting on the swimmer body. A vast majority of living organisms are found to perform motion at microscopic scales, where the viscous forces strongly dominate the motion at low Reynold's number. The Reynolds number in such regimes is of the order of 10^{-4}. To get a comparative idea of this number, the Reynolds number for a human swimming in water is of the order of 10^4, for a Goldfish swimming in water it is of the order of 10^2, and that for a human trying to swim in honey it is of the order of 10^{-3} [7], [8].

There has been a lot of research and a growing interest in exploring new and efficient ways to generate motion at these micro scales, see [5], [9], [10], [11]. Understanding the physics of locomotion in microbes provides many insights. Organisms such as paramecia are covered with cilia that are used much like little oars to synchronously row through water. Motile bacteria use one or more flagella, which are long helical filaments that extend from the cell membrane and act as a propeller. Escherichia Coli is a bacteria commonly found in the lower intestines of humans which, for example, uses such mechanism to swim at 35 diameters per second [12]. Figures 1 and 2 show few such microbes with flagella. In the field of engineering, microbotics (or microrobotics) is one of the recently evolving fields in mobile robots with characteristic dimensions to the scale of a micron. Figure 3 shows an example of a flagellar microswimmer developed at Monash University. Cell or microbial locomotion being an essential part of biological systems, understanding of the means of locomotion is also of a great interest to biologists community. A better understanding of the mechanism of swimming can lead to many useful applications in several fields such as targeted drug delivery, non-evasive surgery, micro-machining and nano technology.

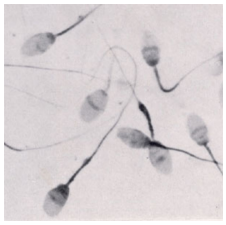

Fig. 1: Sperm cells [13]

Fig. 2: Spirillum bacteria [14]

The slender-body theory and the resistive force theory form the basis for modelling of the fluid forces acting on the systems in this regime [16]. These are used to obtain a relationship between the velocity of the body at each point along its length and the force per unit length experienced by the body at that point. Moreover, the resistive force theory allows us to treat

Sudin Kadam and Ravi Banavar are with Systems and Control Engineering Department, Indian Institute of Technology Bombay, Mumbai, 400076 India e-mail: sudin@sc.iitb.ac.in, banavar@iitb.ac.in

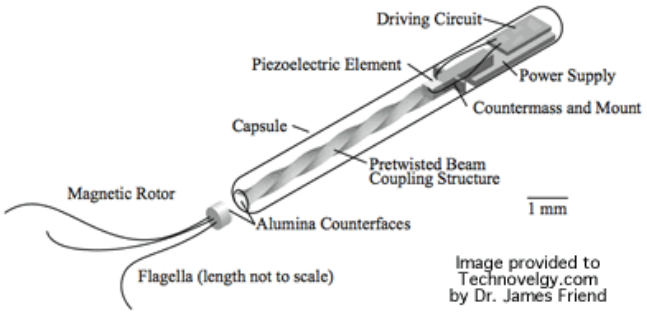

Fig. 3: A flagellum propelled microbot [15]

the forces acting on the individual limbs independent of the motion of the rest of the motion of the other parts of the locomoting body [17]. These features greatly simplify the fluid mechanistic modelling.

From modelling and controls perspective, the locomotion of articulated mechanical systems is often complex. Classical mechanics tends to become intractable for such systems, and tends not to reveal the topological structure of the systems' configurations, velocities and other quantities. Geometric mechanics and control theory aid considerably in the analysis of robotic and animal locomotion, where the treatment of the configuration space as a differentiable manifold allows one to extend the calculus to topological spaces which are not Euclidean [18], [19], [20], [21], [22]. For a large class of locomotion systems, including underwater vehicles, fishlike swimming, flapping winged vehicles, spacecraft with rotors and wheeled or legged robots, it is possible to model the motion using the mathematical structure of a connection on a principal bundle, see [20], [23], [24] for examples.

In his famous lecture on Life at Low Reynolds Number [25], E. M. Purcell presented the simplest swimmer that can effectively propel itself at low Reynolds numbers. This swimmer can be considered as a simplified flagellum made of three slender rods articulated at two hinges. This model gave rise to a lot of research in modelling, control, optimal gait design etc. of this swimmer, see [3], [7], [26], [27], [28], [29], [30], [31] and the references therein. [17] analyzes its locomotion problem in geometric framework, again for the planar case, which uses the low Reynold's number regime and slenderness of the links in mechanism to get a kinematic form of equations. The Cox theory at low Reynold's number for slender bodies is not restricted to planar motion. We extend existing work to a more general, more challenging and more practical 3 dimensional locomotion problem by using tools from geometric mechanics.

A. Contribution:

As mentioned before, the existing literature presents various aspects of modelling and control of the planar Purcell's swimmer. Since microbial and biomimetic motion is certainly not restricted to a plane and evolves in 3 dimensional space, there is a need to study and analyze a 3D model. To our knowledge, this is the first study of a 3 link swimming mechanism which performs generic 3 dimensional motion. Furthermore, by adopting a geometric approach, we identify certain structures in the configuration space which leads to an insightful model for a complex system. Such a geometric approach for the planar Purcells swimmer is given in [32]. We derive a coordinate free expression of the local connection form which avoids the cumbersome notation of local parametrizations right from the onset in modelling. We then present a simulation for a particular gait of the outer limbs and show evolution of the swimmer's motion. This is followed by a local controllability analysis at a particular configuration which characterizes the allowable group motions of the swimmer.

B. Organization of paper:

The paper is organized as follows. In the next section we present the geometry that typical locomotion systems admit, followed by that of the proposed generalized Purcell's swimmer. In section 3, we derive a coordinate-free expression for the principal kinematic form of the swimmer using the Cox and resistive force theories. Section 4 shows results of open loop motion simulation of the swimmer under a specified sinusoidal limb motion. In section 6, we present the local controllability analysis of the swimmer.

II. Construction and the geometry of configuration space

While studying the problem of locomotion using limb motion or shape change, the geometry of the configuration space, which is a differential manifold requires attention for elegant and insightful solutions. The configuration space is written as the product of two manifolds. One part is the base manifold M which describes the configuration of the internal shape variables of the mechanism. The other part depicting the macro-position of the locomoting body is a Lie group G and represents gross displacement of the body. The total configuration space of the robot Q then naturally appears as a product $G \times M$. Such systems follow the topology of a trivial principal fiber bundle, see [33]. Figure 4 shows an explanatory figure of a fiber bundle. With such a separation of the configuration space, locomotion is readily seen as the means by which changes in shape affect the macro position. We refer to [1], [22] for a detailed explanation on the topology of locomoting systems.

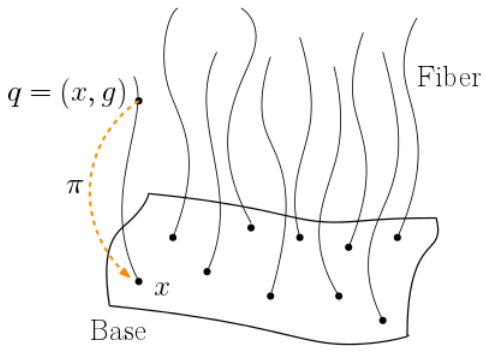

Fig. 4: Fiber Bundle

A. Generalized Purcell's swimmer

The original form of the Purcell's swimmer has three links moving in a plane, the outer links are actuated through a hinge joint with the central or base link such that the mechanism always performs motion in a plane. The details of construction, configuration manifold and the kinematic modelling of this swimmer can be referred from [17]. Fig. 6 shows a schematic of the proposed generalization. We replace the two hinge joints by ball joints, thus allowing out-of-plane shape of the mechanism through yaw, pitch and roll motions of the 2 outer limbs. The middle or base link manoeuvres in the Special Euclidean group $SE(3)$. The translational position of the central (base) link denotes the position of its center and is an element of $\mathbb{R}^3$, and its rotational position is an element of the Special Orthogonal group of matrices $SO(3)$. Each link in our swimmer is modelled as a rigid slender body of length $2L$. The orientation of each of the two outer links also evolve on $SO(3)$. Hence the total configuration space of the proposed swimmer is given by $Q = SO(3) \times SO(3) \times SE(3)$

Definition : *For Q a configuration manifold and G a Lie group, a trivial principal fiber bundle with base M and structure group G is a manifold $Q = M \times G$ with a free left action of G on Q given by left translation in the group variable: $\phi_h(x, g) = (x, hg)$ for $x \in M$ and $g \in G$* [1]

The structure group in our case is $G = SE(3)$. and the shape space M is $SO(3) \times SO(3)$. Since all the points $q \in Q$ are represented by (x, g) with $x \in M$ and $g \in G$, Q has global product structure of the form $M \times G$. Moreover, $SE(3)$ acts via the left action as a matrix multiplication, and has a single identity element, which is a 4×4 identity matrix. Hence left action of the group, defined by $\Phi_h : (x, g) \in Q \longrightarrow (x, hg)$ is free, for $x \in M$ and $h, g \in G$. Thus, the configuration space of the basic Purcell's swimmer satisfies the trivial principal fiber bundle structure.

III. Kinematic Model of the Swimmer

A. Fluid Forces

Due to assumption of low Reynold's number regime, the hydrodynamics of the system is governed by the Stokes equations, which are the simplified Navier-Stokes equations [34]. For a slender body at low Reynold's number, Cox theory gives a linear dependence of forces on velocities, see [16] . This implies that for a slender link of length l, radius a, fluid viscosity μ at speed u the forces acting are given by

$$F_{long} = \frac{2\pi\mu l u_{long}}{ln(\frac{l}{a})} = k_T u_{long} \quad \text{(Along the link length)}$$

$$F_{lat} = \frac{4\pi\mu l u_{lat}}{ln(\frac{l}{a})} = 2k_T u_{lat} \quad \text{(Perpendicular to the link length)}$$

where k_T is the differential viscous drag constant corresponding to translational motion. We model each of the three links of the swimmer as slender members leading to the form of fluid forces' according to Cox theory. We regard the flows around each link as independent of the other links' motions according to resistive force theory [26]. We denote by $\xi_{i,x}$ the translational velocity along the longitudinal axis, and by $\xi_{i,y}$, $\xi_{i,z}$ the translational velocities along the 2 lateral axes of the i'th link. Similarly, $\xi_{i,\omega_x}, \xi_{i,\omega_y}$ and ξ_{i,ω_z} denote angular velocities about the respective 3 body axes of the i'th link. Thus, the total forces and moments acting on the i'th link of length $2L$, in its own frame take the following form

$$\begin{aligned} F_{i,x} &= \int_{-L}^{L} \frac{1}{2} k_T \xi_{i,x} dL = k_T \xi_{i,x} L \\ F_{i,y} &= \int_{-L}^{L} k_T \xi_{i,y} dl = 2k_T \xi_{i,y} L \\ F_{i,z} &= \int_{-L}^{L} k_T \xi_{i,z} dl = 2k_T \xi_{i,z} L \end{aligned}$$

The moments about the center of the link due to rotation about an axis transverse to link is found by taking the lateral drag forces as linearly varying along the link according to its angular velocity. Note that the Cox theory is restricted to forces

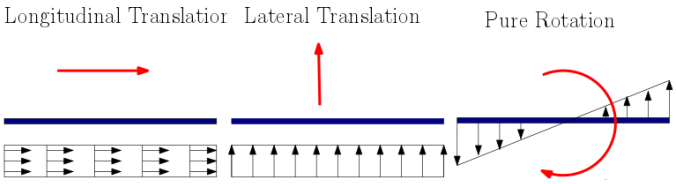

Fig. 5: Force and moments on a slender member

and moment acting on the body performing only translational motion. Thus, to account for the torque acting on a slender link due to spinning about its own axis, we define K_R as the resistive torque per unit length per unit spin speed. Thus, we have total moments as

$$\begin{aligned} M_i &= \int_{-L}^{L} [k_R \xi_{i,\omega_x},\ k_T l^2 \xi_{i,\omega_y},\ k_T l^2 \xi_{i,\omega_z}]^T dl \\ &= [k_R L \xi_{i,\omega_x},\ \frac{2}{3} k_T L^3 \xi_{i,\omega_y},\ \frac{2}{3} k_T L^3 \xi_{i,\omega_z}]^T \end{aligned}$$

Thus, the total forces and moments on each link can be written as linear equation in its body velocities -

$$F_i = \begin{bmatrix} k_T L & 0 & 0 & 0 & 0 & 0 \\ 0 & 2k_T L & 0 & 0 & 0 & 0 \\ 0 & 0 & 2k_T L & 0 & 0 & 0 \\ 0 & 0 & 0 & k_R L & 0 & 0 \\ 0 & 0 & 0 & 0 & \frac{2}{3} k L_T^3 & 0 \\ 0 & 0 & 0 & 0 & 0 & \frac{2}{3} k L_T^3 \end{bmatrix} \begin{pmatrix} \xi_{i,x} \\ \xi_{i,y} \\ \xi_{i,z} \\ \xi_{i,\omega_x} \\ \xi_{i,\omega_y} \\ \xi_{i,\omega_z} \end{pmatrix}$$

Which, for the i^{th} link can be simply written as

$$F_i = H_i \xi_i \tag{1}$$

B. Coordinate frames and transformations

Fig 7 shows an arbitrary position of the system along with 3 coordinate frames corresponding to each link. The frame corresponding to base link has its origin at its geometric center, whereas the frames corresponding to the outer links are at their respective joints with base link. The orientation of the outer links is represented using an element of Special Orthogonal group of 3×3 matrices. Thus $R_1, R_2 \in SO(3)$ define the

coordinates of the shape space M. The reference configuration is the one in which all the 3 coordinate frames are aligned to each other, i.e. R_1 and R_2 both are the identity matrices.

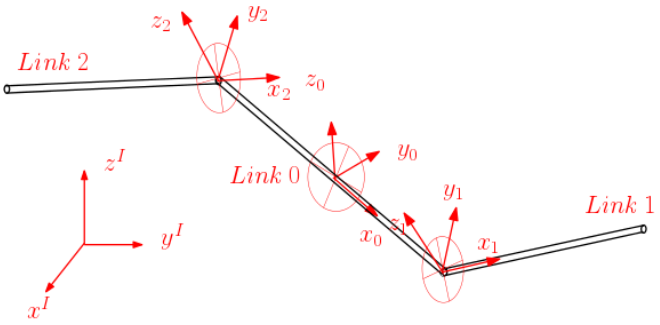

Fig. 6: Generalized Purcell's swimmer configuration

We write the kinematics of the i'th link in terms of the velocity of the base link ξ_0 and the angular velocities of the 2 outer links. The velocity of i'th link in its own body frame is an element of the Lie algebra $\mathfrak{g}$, which in our case is $se(3)$. It is represented as a generalized velocity vector by an element of $\mathbb{R}^6$ as $\xi_i = \left[\xi_{i,x},\ \xi_{i,y},\ \xi_{i,z},\ \xi_{i,\omega_x},\ \xi_{i,\omega_y},\ \xi_{i,\omega_z}\right]^T$.

C. Construction of the connection form

A mechanical system having a principal fiber bundle structure and group symmetry in Lagrangian can be shown to satisfy the general reconstruction equation

$$\xi = -A(r)\dot{r} + \mathbb{I}^{-1}p \tag{2}$$

where, for a shape manifold M, its tangent space at a point $r \in M$ is denoted by T_rM, the local connection form is $A(r) : T_rM \longrightarrow \mathfrak{g}$, $\mathbb{I} : \mathfrak{g} \longrightarrow \mathfrak{g}^*$ is the locked inertia tensor and $p \in \mathfrak{g}^*$ is the generalized momentum of the system, see [4], [18] for details on kinematic systems. For swimming at low Reynolds number, the strong dominance of viscous forces means that the momentum terms drops out. Thus, the reconstruction equation takes the following kinematic form

$$\xi = -A(r)\dot{r} \tag{3}$$

In the following part of the paper, we obtain a model of the 3 dimensional Purcell's swimmer in this kinematic form. In order to derive the force on each link, from equation 1, we see that we need to find the body velocity of each link in terms of the body velocity of the base link and the shape velocities $\omega_1 = \left[\xi_{1,\omega_x},\ \xi_{1,\omega_y},\ \xi_{1,\omega_z}\right]^T$ and $\omega_2 = \left[\xi_{2,\omega_x},\ \xi_{2,\omega_y},\ \xi_{2,\omega_z}\right]^T$, which are the angular velocities of links 1 and 2 respectively in their own frames. ω_1, ω_2 also constitute the inputs to our kinematic system. The relationship between body and shape velocities is obtained for link 1 as

$$\begin{aligned}\xi_1 &= \begin{bmatrix} R_1 & -\begin{bmatrix} l \\ 0 \\ 0 \end{bmatrix}^{\times} & 0_{3\times3} & 0_{3\times3} \\ 0 & R_1 & e_{3\times3} & 0_{3\times3} \end{bmatrix} \begin{pmatrix} \xi_0 \\ \omega_1 \\ \omega_2 \end{pmatrix} \\ &= B_1 \begin{pmatrix} \xi_0 \\ \omega_1 \\ \omega_2 \end{pmatrix}\end{aligned} \tag{4}$$

where $0_{3\times3}$ and $e_{3\times3}$ are zero and identity matrices of size 3×3, respectively. The hat map $(.)^{\times}$ is defined in appendix. A similar expression can be derived for the second link as

$$\begin{aligned}\xi_2 &= \begin{bmatrix} R_2 & \begin{bmatrix} l \\ 0 \\ 0 \end{bmatrix}^{\times} & 0_{3\times3} & 0_{3\times3} \\ 0 & R_2 & 0_{3\times3} & e_{3\times3} \end{bmatrix} \begin{pmatrix} \xi_0 \\ \omega_1 \\ \omega_2 \end{pmatrix} \\ &= B_2 \begin{pmatrix} \xi_0 \\ \omega_1 \\ \omega_2 \end{pmatrix}\end{aligned} \tag{5}$$

This leads us to the following form of the velocity of each of links 0, 1 and 2

$$\xi_0 = \begin{pmatrix} \xi_{0,x} \\ \xi_{0,y} \\ \xi_{0,z} \\ \xi_{0,\omega_x} \\ \xi_{0,\omega_y} \\ \xi_{0,\omega_z} \end{pmatrix}, \qquad \xi_1 = B_1 \begin{pmatrix} \xi_0 \\ \omega_1 \\ \omega_2 \end{pmatrix}, \qquad \xi_2 = B_2 \begin{pmatrix} \xi_0 \\ \omega_1 \\ \omega_2 \end{pmatrix} \tag{6}$$

Next, from fluid force equations (1), we see that the force on each link is linearly dependent on the velocity of the link in its own frame. Hence the force on each of the 3 links is

$$F_0 = H_0\xi_0,\ F_1 = H_1B_1 \begin{pmatrix} \xi_0 \\ \omega_1 \\ \omega_2 \end{pmatrix},\ F_2 = H_2B_2 \begin{pmatrix} \xi_0 \\ \omega_1 \\ \omega_2 \end{pmatrix} \tag{7}$$

The summation of all the forces gives us the resultant force acting on the system. But we note that equation (1) gives us the force with respect to the frame of the respective link. Hence before summing up, we transform the forces to the frame associated with base link as follows

$$F^0_{net} = F_0 + T^0_1F_1 + T^0_2F_2 \tag{8}$$

where the transformation matrices corresponding to outer links are

$$T^0_1 = \begin{bmatrix} R_1^T & 0 \\ \begin{bmatrix} l \\ 0 \\ 0 \end{bmatrix}^{\times} R_1^T & R_1^T \end{bmatrix}, \qquad T^0_2 = \begin{bmatrix} R_2^T & 0 \\ \begin{bmatrix} -l \\ 0 \\ 0 \end{bmatrix}^{\times} R_2^T & R_2^T \end{bmatrix} \tag{9}$$

We substitute the forces on each link using equations 1 and 6 and then split these equations by writing matrices in terms of their block format as

$$\begin{aligned} F &= H_0\xi_0 + T^0_1H_1B_1 \begin{pmatrix} \xi_0 \\ \omega_1 \end{pmatrix} + T^0_2H_2B_2 \begin{pmatrix} \xi_0 \\ \omega_2 \end{pmatrix} \\ &= H_0\xi_0 + [[T^0_1H_1B_1]_{6\times6}\ \ [T^0_1H_1B_1]_{6\times3}] \begin{pmatrix} \xi_0 \\ \omega_1 \end{pmatrix} \\ &\quad + [[T^0_2H_2B_2]_{6\times6}\ \ [T^0_2H_2B_2]_{6\times3}] \begin{pmatrix} \xi_0 \\ \omega_2 \end{pmatrix} \end{aligned}$$

The consequence of being at low Reynolds number is that the net forces and moments on an isolated system should be zero,

which leads to following equation

$$0 = H_0\xi_0 + [T_1^0 H_1 B_1]_{6\times 6}\,\xi_0 + [T_1^0 H_1 B_1]_{6\times 3}\,\omega_1 + [T_2^0 H_2 B_2]_{6\times 6}\,\xi_0 + [T_2^0 H_2 B_2]_{6\times 3}\,\omega_2$$

Finally, by rearranging we get a kinematic form of reconstruction equation as

$$\xi_0 = -P^{-1}Q\,\dot{r} \tag{10}$$

where $\dot{r} = [\omega_1,\ \omega_2]^T$ is the vector of shape velocities. P and Q matrices are given as follows

$$P = [H_0 + [T_1^0 H_1 B_1] + [T_2^0 H_2 B_2]]_{6\times 6} \text{ and}$$
$$Q = [[T_1^0 H_1 B_1]_{6\times 2} \quad [T_2^0 H_2 B_2]_{6\times 2}]_{6\times 4}$$

This is the desired model in a kinematic form, $\xi = -A(r)\dot{r}$, where $A(r)$ is the local connection form defined at each $r = (R_1, R_2) \in M = SO(3) \times SO(3)$ and the shape velocity $\dot{r} = [\omega_1,\ \omega_2]^T \in T_rM$. For the proposed 3 dimensional Purcell's swimmer, the local connection form $A(r)$ is a 6×6 matrix, and it depends on the lengths of the limbs, viscous drag coefficients k_T, k_R and the shape of the mechanism r. In our example the Lie group is the Special Euclidean group $SE(3)$, and $\xi = [v_x, v_y, v_z, \omega_x, \omega_y, \omega_z]^T$ belongs to its tangent space at the identity. The connection form and the other notions mentioned here have roots in geometric mechanics, see [18], [19] for details.

IV. Simulation Results

In this section, we present results of the simulation we performed for the 3D Purcell's swimmer given in equation 10 for a specified profile of the outer limbs' motion. For simulation purpose we assign coordinates to our configuration manifold as shown in figure 7 and described as follows

- We identify the motion of the outer limbs as that evolving on 2-sphere $\mathbb{S}^2 \subset SO(3)$. This means that there is no actuation for the outer limbs about their respective longitudinal axes.
- We have 2 coordinates θ, ϕ representing the orientation of the outer links with respect to base link
- Orientation of any of the outer links can be represented with respect to the base link using the composite rotation $R_y^\phi R_z^\theta$, where

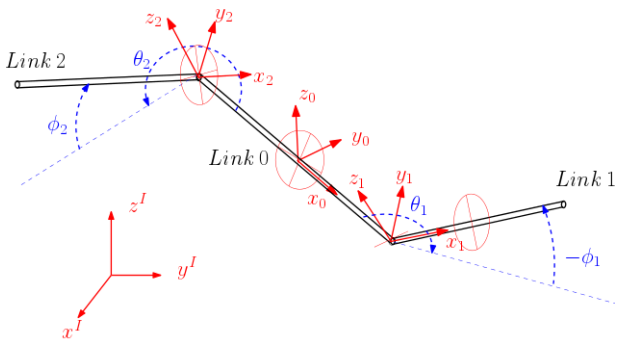

Fig. 7: Generalized Purcell's swimmer configuration

$$R_z^\theta = \begin{bmatrix} \cos\theta & \sin\theta & 0 \\ -\sin\theta & \cos\theta & 0 \\ 0 & 0 & 1 \end{bmatrix}, R_y^\phi = \begin{bmatrix} \cos\phi & 0 & -\sin\phi \\ 0 & 1 & 0 \\ \sin\phi & 0 & \cos\phi \end{bmatrix}$$

- The base link's translation position and velocity is described with respect to the inertial frame
- The parametrization of orientation $R \in SO(3)$ of the base link with respect to the inertial frame is done using a z-y-x sequence of Euler angles γ, β, α, such that the orientation of the base link with respect to the inertial frame $R_0^{\mathcal{I}}$ is obtained as

$$R_0^{\mathcal{I}} = R_x(\alpha)R_y(\beta)R_z(\gamma) \tag{11}$$

where $R_x(\alpha), R_y(\beta), R_z(\gamma)$ denote rotations about z, y and x axis of the current frames in composite rotations.

We show the relevant terms involved in the derivation of the kinematic equation for the local parametrization of the outer limbs' orientation by angles θ_1, θ_2, ϕ_1 and ϕ_2. The transformation matrices appearing in equations 9 become as

$$T_1^0 = \left[\begin{array}{c|c} R_z^{-\theta_1} R_y^{-\phi_1} & 0 \\ \hline \begin{bmatrix} L + L\cos\phi_1\cos\theta_1 \\ L\cos\phi_1\sin\theta_1 \\ L\sin\phi_1 \end{bmatrix}^\times R_z^{-\theta_1} R_y^{-\phi_1} & R_z^{-\theta_1} R_y^{-\phi_1} \end{array}\right]$$

$$T_2^0 = \left[\begin{array}{c|c} R_z^{-\theta_2} R_y^{-\phi_2} & 0 \\ \hline \begin{bmatrix} L + L\cos\phi_2\cos\theta_2 \\ L\cos\phi_2\sin\theta_2 \\ L\sin\phi_2 \end{bmatrix}^\times R_z^{-\theta_2} R_y^{-\phi_2} & R_z^{-\theta_2} R_y^{-\phi_2} \end{array}\right]$$

The B matrices in equation 4, 5 relating group and joint velocities to outer limbs' velocities in their own frame appear in the following form for the outer link 1 as $B_1 = \begin{bmatrix} B^{11} & B^{12} & B^{13} \\ B^{21} & B^{22} & B^{23} \end{bmatrix}$

$$B^{11} = R_y^{\phi_1} R_z^{\theta_1}, \qquad B^{12} = -B^{11} \begin{bmatrix} L + L\cos\phi_1\cos\theta_1 \\ L\cos\phi_1\sin\theta_1 \\ L\sin\phi_1 \end{bmatrix}^\times,$$

$$B^{13} = \begin{bmatrix} 0 & 0 \\ L\cos\phi_1 & 0 \\ 0 & L \end{bmatrix}, \quad B^{21} = 0_{3\times 3},$$

$$B^{22} = R_y^{\phi_1} R_z^{\theta_1}, \qquad B^{23} = \begin{bmatrix} \sin\phi_1 & 0 \\ 0 & 1 \\ \cos\phi_1 & 0 \end{bmatrix}$$

A similar expression is obtained for B_2.

The simulation was carried out with link length $L = 0.1m$, slenderness ratio $SR = 0.1$, the fluid was considered to be glycerin which has dynamic viscosity ν of $0.95PaS$. The max angular speed of a link was restricted to $0.5\ deg/s$, which gives a Reynolds number to the order of 10^{-4}. Hence Cox theory is applicable, and we used viscous drag coefficients by the method described in section III. The joint velocities were given as inputs having following time parametrization

- Joint 1 :

$$\theta_1 = 20\sin(\frac{1}{40} \times t)\ deg, \qquad \phi_1 = 5\cos(\frac{1}{40} \times t)\ deg,$$
$$\dot{\theta}_1 = \frac{20}{40}\cos(\frac{1}{40} \times t)\ deg/s, \qquad \dot{\phi}_1 = \frac{-5}{40}\sin(\frac{1}{40} \times t)\ deg/s$$

- Joint 2 :

$$\theta_2 = 20\sin(\frac{-1}{40} \times t)\ deg, \qquad \phi_2 = 5\sin(\frac{1}{40} \times t)\ deg,$$
$$\dot{\theta}_2 = -\frac{20}{40}\cos(\frac{-1}{40} \times t)\ deg/s, \qquad \dot{\phi}_2 = \frac{5}{40}\cos(\frac{1}{40} \times t)\ deg/s$$

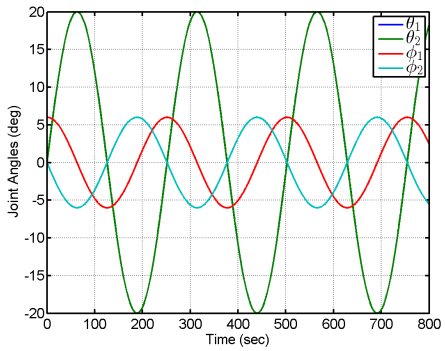

Fig. 8: Joint positions

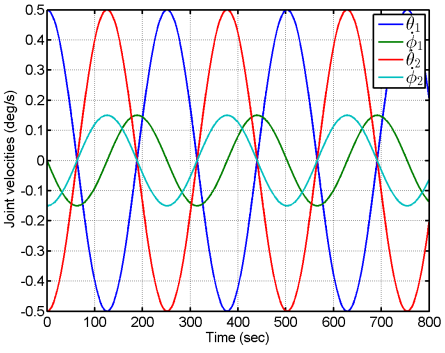

Fig. 9: Joint velocities

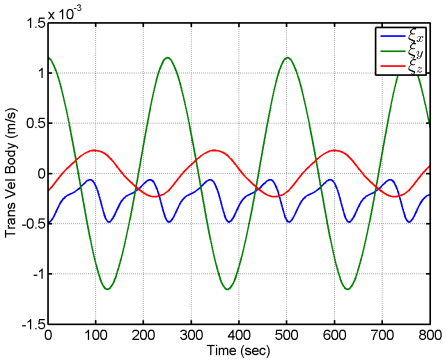

Fig. 10: Base link translational velocities

Figures 8 to 13 show the temporal variation translation and angular position and velocities for above mentioned joint actuation parametrization for a period of 840 seconds. Figures 14 to 21 show various shapes and the net displacement of the mechanism in 3 dimensional space across timeframes separated by 100 seconds.

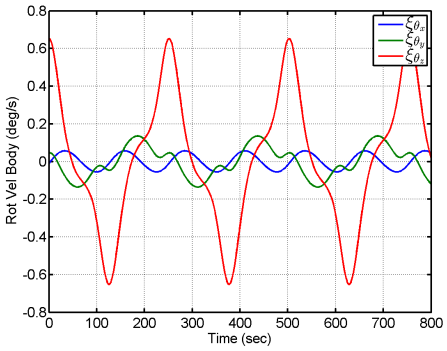

Fig. 11: Base link Rotational velocities

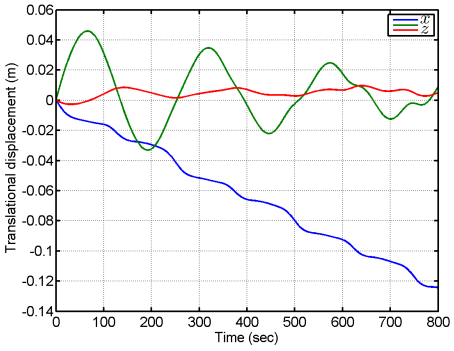

Fig. 12: Base link Translational displacement

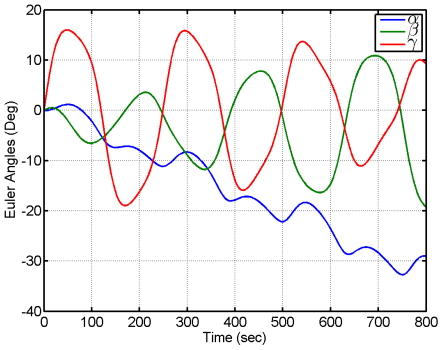

Fig. 13: Base link Euler Angles' variation

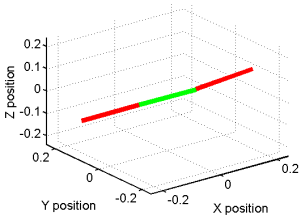

Fig. 14: Time = 0seconds

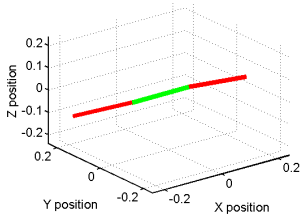

Fig. 15: Time = 120seconds

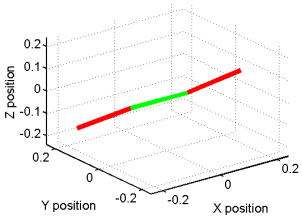

Fig. 16: Time = 240seconds

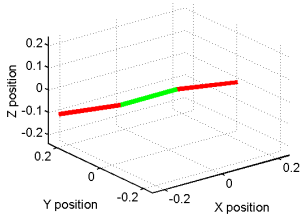

Fig. 17: Time = 360seconds

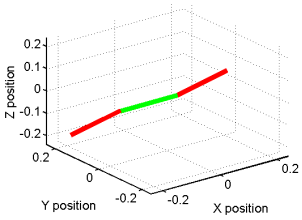

Fig. 18: Time = 480seconds

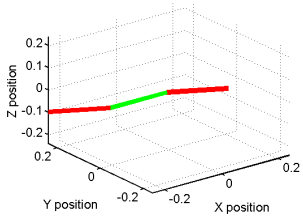

Fig. 19: Time = 600seconds

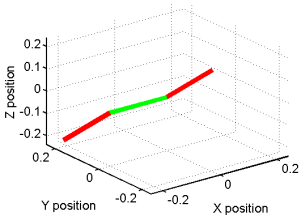

Fig. 20: Time = 720seconds

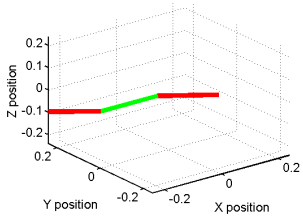

Fig. 21: Time = 840seconds

V. Local controllability analysis

The overall kinematics of the swimmer can be written in the form of a nonlinear linear-in-control system as

$$\begin{bmatrix} \dot{r} \\ \xi \end{bmatrix} = \begin{bmatrix} e_{4\times4} \\ -A(r) \end{bmatrix} \dot{r} \tag{12}$$

where, $e_{4\times4}$ is a 4×4 identity matrix and $\dot{r} = [\dot{\theta}_1, \dot{\theta}_2, \dot{\phi}_1, \dot{\phi}_2]^T \in T_rM$ is the control input. The use of Chow's theorem to comment on the local controllability of this system requires us to check the Lie algebra rank condition of the control vector fields [35], [36]. We tried to do this for the 3D Purcell's swimmer for a configuration where all the 3 links are collinear with each other. The first step is to check the rank of A at the given configuration, and it was observed that the rank of the connection form A is 4 at this configuration.

$$A(0,0,0,0) = \begin{bmatrix} 0 & 0 & 0 & 0.33 \\ 3.44 & 0 & 2.77 & 0 \\ 0 & -3.44 & 0 & 0 \\ 0 & 0 & 0 & -0.44 \\ 0 & 2.33 & 0 & 0.33 \\ 2.33 & 0 & 2.33 & 0 \end{bmatrix} \tag{13}$$

But computing the Lie algebra of the control vector fields requires calculation of successive Lie brackets, which requires the explicit form of these vector fields. Due to the matrix inversion step involved (see equation 10), the expression for these vector fields becomes extremely bulky, which, consequently, makes Lie bracket calculation computationally highly intensive. Moreover, in the midst of such bulky terms, the physical insight into the system gets lost. Thus, we have used an alternate and indirect approach based on the controllability results of the planar Purcell's swimmer to comment on the local weak controllability of the proposed 3D swimmer.

The principal fiber bundle structure in the controllability analysis naturally gives rise to a finer notion of weak controllability. For such systems a point in the configuration space is written as $q = (r, g) \in M \times G = Q$. For a curve $r(t) \in M$, the horizontal lift $r^*(t) \in Q$ is a curve which projects to $x(t)$ under the projection map defining the principal fiber bundle and the components of its tangent vectors $\dot{r}^*(t) \in T_qQ$ satisfy the reconstruction equation (10). Then a locomotion system is said to be weakly controllable if, for any initial position $g_0 \in G$, and final position $g_f \in G$, and initial shape $r_0 \in M$, there exists a time $T > 0$ and a curve in the base space $r(t)$ satisfying $r(0) = r_0$ such that the horizontal lift of $r(t)$ passing through (r_0, g_0) satisfies $r^*(0) = q_0$ and $r^*(T) = (r(T), g_f)$.

Then, given the following vector spaces,

$$\begin{aligned}
\mathfrak{h}_1 &= span\{A(x)(X) : X \in T_xM\}, \\
\mathfrak{h}_2 &= span\{DA(x)(X,Y) : X, Y \in T_xM\}, \\
\mathfrak{h}_3 &= span\{L_Z DA(x)(X,Y) - [A(x)(Z), DA(x)(X,Y)], \\
&\qquad [DA(x)(X,Y), DA(x)(W,Z)] : W, X, Y, Z \in T_xM\} \\
&\vdots \\
\mathfrak{h}_k &= span\{L_X \xi - [A(x)(X), \xi], [\eta, \xi] : X \in T_xM, \\
&\qquad \xi \in \mathfrak{h}_{k-1}, \eta \in \mathfrak{h}_2 \oplus \cdots \oplus \mathfrak{h}_{k-1}\}
\end{aligned}$$

Then, a system defined on a trivial principal bundle Q is locally weakly controllable near $q \in Q$ if and only if the space of the Lie algebra $\mathfrak{g}$ of the structure group G is spanned by the vector fields $\mathfrak{h}_1, \mathfrak{h}_2, \cdots$ as follows

$$\mathfrak{g} = \mathfrak{h}_1 \oplus \mathfrak{h}_2 \oplus \cdots$$

This idea of weak controllability is also of practical relevance since often just reaching the desired group component without strict requirement on shape of the system is sufficient. We make use of the controllabilty results from [37], [38], which state that the original planar Purcell's swimmer is controllable at this collinear configuration. We decompose the limb motion of the 3D swimmer into that of 2 planar swimmers as shown in the figures 22, 23, and use the result that in each of these

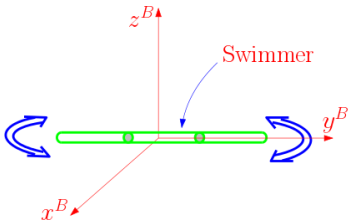

Fig. 22: Limb motion in XY plane

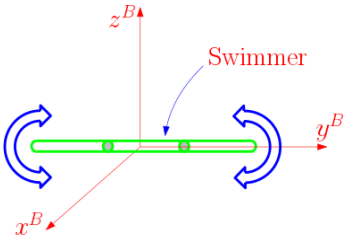

Fig. 23: Limb motion in YZ plane

planes the planar swimmer's motion on $SE(2)$ group is locally fully controllable.

Since the 3D swimmer's limbs are actuated in both the X-Y and Y-Z planes, the planar Purcell's swimmer's controllability results imply that,

- For the case of limb actuation in X-Y plane ($\phi_1 = \phi_2 = 0$), the swimmer's translational motion is locally controllable in the X and Y axis directions, and the rotational motion about the Z axis is controllable.
- For the case of limb actuation in Y-Z plane ($\theta_1 = \theta_2 = 0$), the swimmer's translational motion is locally controllable in the Y and Z axis directions, and the rotational motion about the X axis is controllable.

Thus, at this collinear configuration, we say that the swimmer is at least weakly controllable for its translational motion along all the 3 orthogonal axes, and for its rotation about 2 orthogonal axes transverse to the base link's axis.

VI. Conclusion

This paper introduced a generalized version of the Purcell's swimmer which performs 3 dimensional motion. We highlight the topology of a trivial principal fiber bundle that the configuration space of this swimmer inherits, and derive a kinematic form of equations by utilizing the properties at low Reynold's number regime. Matrix Lie groups are used in order to get a coordinate free expression of the local connection form. We then use a local parametrization for a restricted actuation of the outer limbs on a sphere $\mathbb{S}^2$ to generate a set of simulation results. A local nonlinear controllability of the 3D swimmer was studied based on the weak controllability results of the planar Purcell's swimmer. The decomposition of the limb motion of the 3D swimmer in 2 orthogonal planes has been utilized to understand the achievable group motions of the swimmer's base link. An interesting avenue of research is to explore optimal control and motion planning strategies for the 3D swimmer presented here. We hope to work on these issues in the future.

Acknowledgment

A part of this work was accomplished by the second author during his tenure as a Pratt and Whitney Chair Professor in the Department of Aerospace Engineering, Indian Institute of Science.

Appendix A

Hat map of an n dimensional vector maps it to $n \times n$ a skew symmetric matrix. In this work, hat map of 3 dimensional vector is used which takes the following form

$$\begin{bmatrix} a \\ b \\ c \end{bmatrix}^{\times} = \begin{bmatrix} 0 & -c & b \\ c & 0 & -a \\ -b & a & 0 \end{bmatrix}$$

The hat map is useful in writing a cross product of 2 vectors x, y compactly as a matrix multiplication -

$$x \times y = x^{\times} y = -y^{\times} x$$

References

[1] S. D. Kelly and R. M. Murray, "Geometric phases and robotic locomotion," *Journal of Robotic Systems*, vol. 12, no. 6, pp. 417–431, 1995.

[2] K. Morgansen, B. Triplett, D. J. Klein *et al.*, "Geometric methods for modeling and control of free-swimming fin-actuated underwater vehicles," *Robotics, IEEE Transactions on*, vol. 23, no. 6, pp. 1184–1199, 2007.

[3] J. B. Melli, C. W. Rowley, and D. S. Rufat, "Motion planning for an articulated body in a perfect planar fluid," *SIAM Journal on applied dynamical systems*, vol. 5, no. 4, pp. 650–669, 2006.

[4] E. A. Shammas, H. Choset, and A. A. Rizzi, "Geometric motion planning analysis for two classes of underactuated mechanical systems," *The International Journal of Robotics Research*, vol. 26, no. 10, pp. 1043–1073, 2007.

[5] R. Dreyfus, J. Baudry, M. L. Roper, M. Fermigier, H. A. Stone, and J. Bibette, "Microscopic artificial swimmers," *Nature*, vol. 437, no. 7060, pp. 862–865, 2005.

[6] S. Childress, *Mechanics of swimming and flying*. Cambridge University Press, 1981, vol. 2.

[7] A. Najafi and R. Golestanian, "Simple swimmer at low reynolds number: Three linked spheres," *Physical Review E*, vol. 69, no. 6, p. 062901, 2004.

[8] N. Cohen and J. H. Boyle, "Swimming at low reynolds number: a beginners guide to undulatory locomotion," *Contemporary Physics*, vol. 51, no. 2, pp. 103–123, 2010.

[9] L. E. Becker, S. A. Koehler, and H. A. Stone, "On self-propulsion of micro-machines at low reynolds number: Purcell's three-link swimmer," *Journal of fluid mechanics*, vol. 490, pp. 15–35, 2003.

[10] T. Qiu, T.-C. Lee, A. G. Mark, K. I. Morozov, R. Münster, O. Mierka, S. Turek, A. M. Leshansky, and P. Fischer, "Swimming by reciprocal motion at low reynolds number," *Nature communications*, vol. 5, 2014.

[11] G. Taylor, "Analysis of the swimming of microscopic organisms," in *Proceedings of the Royal Society of London A: Mathematical, Physical and Engineering Sciences*, vol. 209, no. 1099. The Royal Society, 1951, pp. 447–461.

[12] H. C. Berg, *E. coli in Motion*. Springer Science & Business Media, 2008.

[13] S. Lawler, "Sex cells: sperm that crawl instead of swim," $http://theconversation.com/sex-cells-sperm-that-crawl-instead-of-swim-7219$, 2012, [Online; accessed 1-August-2016].

[14] Web, "Look for diagnosis," $https://lookfordiagnosis.com/mesh_info.php?term=spirillumlang=1$, 2016, [Online; accessed 1-August-2016].

[15] technovelgy, "Microrobot to swim like bacteria with flagellar propeller: Science fiction in the news," 2016, online; accessed 13-August-2016. [Online]. Available: "http://www.technovelgy.com/ct/Science-Fiction-News.asp?NewsNum=845"

[16] R. Cox, "The motion of long slender bodies in a viscous fluid part 1. general theory," *Journal of Fluid mechanics*, vol. 44, no. 04, pp. 791–810, 1970.

[17] R. L. Hatton and H. Choset, "Geometric swimming at low and high reynolds numbers," *Robotics, IEEE Transactions on*, vol. 29, no. 3, pp. 615–624, 2013.

[18] A. Bloch, "Nonholonomic mechanics," in *Nonholonomic Mechanics and Control*. Springer, 2003, pp. 207–276.

[19] D. D. Holm, T. Schmah, C. Stoica, and D. C. Ellis, *Geometric mechanics and symmetry: from finite to infinite dimensions*. Oxford University Press London, 2009.

[20] J. Ostrowski and J. Burdick, "The geometric mechanics of undulatory robotic locomotion," *The international journal of robotics research*, vol. 17, no. 7, pp. 683–701, 1998.

[21] F. Bullo and A. D. Lewis, *Geometric control of mechanical systems: modeling, analysis, and design for simple mechanical control systems*. Springer Science & Business Media, 2004, vol. 49.

[22] A. M. Bloch, P. Krishnaprasad, J. E. Marsden, and R. M. Murray, "Nonholonomic mechanical systems with symmetry," *Archive for Rational Mechanics and Analysis*, vol. 136, no. 1, pp. 21–99, 1996.

[23] A. Cabrera, "Base-controlled mechanical systems and geometric phases," *Journal of Geometry and Physics*, vol. 58, no. 3, pp. 334–367, 2008.

[24] S. D. K. M. J. Fairchild and P. M. H. P. Tallapragada, "Proportional heading control for planar navigation: The chaplygin beanie and fishlike robotic swimming," *energy*, vol. 50, no. 1, p. 2, 2012.

[25] E. M. Purcell, "Life at low reynolds number," *Am. J. Phys*, vol. 45, no. 1, pp. 3–11, 1977.

[26] D. Tam and A. E. Hosoi, "Optimal stroke patterns for purcells three-link swimmer," *Physical Review Letters*, vol. 98, no. 6, p. 068105, 2007.

[27] E. Passov and Y. Or, "Dynamics of Purcell's three-link microswimmer with a passive elastic tail," *The European Physical Journal E*, vol. 35, no. 8, pp. 1–9, 2012.

[28] L. J. Burton, "The dynamics and kinematics of bio-in swimming systems," Ph.D. dissertation, Massachusetts Institute of Technology, 2013.

[29] J. Avron and O. Raz, "A geometric theory of swimming: Purcell's swimmer and its symmetrized cousin," *New Journal of Physics*, vol. 10, no. 6, p. 063016, 2008.

[30] Y. Or, J. Vankerschaver, S. D. Kelly, R. M. Murray, and J. E. Marsden, "Geometric control of particle manipulation in a two-dimensional fluid," in *Decision and Control, 2009 held jointly with the 2009 28th Chinese Control Conference. CDC/CCC 2009. Proceedings of the 48th IEEE Conference on*. IEEE, 2009, pp. 19–26.

[31] J. Lohéac, J.-F. Scheid, and M. Tucsnak, "Controllability and time optimal control for low reynolds numbers swimmers," *Acta Applicandae Mathematicae*, vol. 123, no. 1, pp. 175–200, 2013.

[32] R. L. Hatton and H. Choset, "Connection vector fields for underactuated systems," in *Biomedical Robotics and Biomechatronics, 2008. BioRob 2008. 2nd IEEE RAS & EMBS International Conference on*. IEEE, 2008, pp. 451–456.

[33] S. Kobayashi and K. Nomizu, *Foundations of differential geometry*. New York, 1963, vol. 1, no. 2.

[34] R. L. Hatton, L. J. Burton, A. Hosoi, and H. Choset, "Geometric maneuverability with applications to low reynolds number swimming," in *Intelligent Robots and Systems (IROS), 2011 IEEE/RSJ International Conference on*. IEEE, 2011, pp. 3893–3898.

[35] J.-M. Coron, *Control and nonlinearity*. American Mathematical Soc., 2007, no. 136.

[36] V. Jurdjevic, *Geometric control theory*. Cambridge university press, 1997.

[37] L. Giraldi, P. Martinon, and M. Zoppello, "Controllability and optimal strokes for n-link microswimmer," in *Decision and Control (CDC), 2013 IEEE 52nd Annual Conference on*. IEEE, 2013, pp. 3870–3875.

[38] S. Kadam and R. N. Banavar, "Geometric controllability of the purcells swimmer and its symmetrized cousin," in *Nonlinear Control Systems, 2008. NOLCOS 2016. 10th IFAC Symposium on*. IFAC, 2016, pp. 451–456.